Analysis of longitudinal-field reflection in dielectric gratings

Shayan Mookherjea* and Uriel Levy
University of California, San Diego, Mail Code 0407, La Jolla, California 92093-0407, USA
(Received 24 September 2004; revised manuscript received 19 January 2005; published 20 May 2005)

Because of a common approximation used in the derivation of the wave equation, conventional analyses of Bragg reflection from dielectric gratings do not account for the distinctive behavior of the longitudinal field component of the electric field. We address this issue, which has particular significance in subwavelength scale periodic dielectric structures. We discuss new reflection phenomena within the theoretical framework of coupled-wave analysis, supplemented with numerical calculations.

DOI: 10.1103/PhysRevE.71.056609 PACS number(s): 42.25.Bs, 42.40.Pa, 42.79.Dj, 41.20.Jb

Since any periodic variation in the dielectric coefficient can be decomposed into a Fourier series of linearly superimposed sinusoidal gratings, the analysis of Bragg reflection from sinusoidal dielectric gratings is of fundamental and broad interest. The theory of Bragg reflection is the cornerstone of many research areas in photonics, including diffraction, distributed feedback lasers, optical filtering, grating-enhanced nonlinear optics, and photonic crystals.

Early milestones in the theoretical framework include the coupled-mode theory formulations based on ideal-mode expansion in the colinear geometry [1,2] as well as the analysis of TE-TM mode coupling under conditions of oblique incidence [3]. The subsequent local normal mode expansion methods [4] resulted in more accurate description of the TM reflection coefficient, and the "rigorous coupled-wave theory" (summation over diffraction orders) was introduced [5]. Recent publications include the interaction of forward- and backward-propagating modes in both the TE and TM polarizations—a four-wave problem [6]—and an investigation of thin surface gratings using a technique based on Green's functions [7].

In this paper, we discuss the role of the longitudinal electric field in periodic dielectric structures, and in particular, investigate reflection phenomena. The longitudinal component of the electric field is of recent interest for demonstrated and proposed applications in near-field microscopy, single molecule studies, charged particle accelerators, and ultrafocused light [8–12]. In Sec. I, we present qualitative arguments why investigation of the longitudinal field component may reveal phenomena different from what is conventionally expected, and in Secs. II and III, we present a more detailed theoretical analyses, supplemented with direct numerical calculations of field propagation in the appropriate regime. Section IV discusses the conditions that are necessary to observe these phenomena.

I. INTRODUCTION

In writing the wave equation, one usually makes the approximation that the normalized variation in the dielectric coefficient per unit length $|\nabla \epsilon(\mathbf{r})/\epsilon(\mathbf{r})|$, is much smaller than the corresponding fractional change in the electric field amplitude $|\nabla \cdot \mathbf{E}(\mathbf{r})/\mathbf{E}(\mathbf{r})|$. While justified for macroscopic dielectric structures, this approximation does not hold in general [13,14] and is certainly suspect in subwavelength gratings [15] and similar structures.

The wave equation is derived from Maxwell's equations for the Fourier components at the optical frequency ω of the fields $\mathbf{E}(\mathbf{r},t)=\mathbf{E}(\mathbf{r})\exp(-i\omega t)$ and similarly for $\mathbf{H}(\mathbf{r},t)$ [16]. Without neglecting terms that arise from the divergence condition $\nabla \cdot \epsilon_0 \epsilon(\mathbf{r})\mathbf{E}(\mathbf{r})=0$, we obtain

$$\nabla^2 \mathbf{E}(\mathbf{r}) + \frac{\omega^2}{c^2}\epsilon(\mathbf{r})\mathbf{E}(\mathbf{r}) + \nabla\left(\frac{1}{\epsilon(\mathbf{r})}\mathbf{E}(\mathbf{r})\cdot\nabla\epsilon(\mathbf{r})\right)=0, \quad (1)$$

where $1/c^2 \equiv \mu_0 \epsilon_0$, ϵ_0 is the vacuum permittivity and $\epsilon(\mathbf{r})$ is a dimensionless function describing the spatial variation of the refractive index, e.g., in a uniform medium with refractive index n_0, $\epsilon(\mathbf{r})=n_0^2$. For a one-dimensional grating, $\epsilon(\mathbf{r})=\epsilon(x)$, the third term of Eq. (1) becomes

$$\nabla\left(\frac{1}{\epsilon(\mathbf{r})}\mathbf{E}(\mathbf{r})\cdot\nabla\epsilon(\mathbf{r})\right) \rightarrow \hat{x}\left[-\frac{1}{\epsilon^2}\left(\frac{d\epsilon}{dx}\right)^2 + \frac{1}{\epsilon}\frac{d^2\epsilon}{dx^2}\right]E_x(\mathbf{r}) + \frac{1}{\epsilon}\frac{d\epsilon}{dx}\nabla E_x(\mathbf{r}). \quad (2)$$

A sketch of the geometry is shown in Fig. 1, along with the polarization directions for the waves considered in Secs. II and III. (We set $\partial/\partial y \rightarrow 0$ in all equations, assuming a uniform structure along the y axis.) Clearly, a sinusoidal perturbation in $\epsilon(x)$ of the form $\sin(2\pi x/b)$ will introduce, among others, a term that is spatially varying as $\cos^2(2\pi x/b)$. This term will affect the $\hat{x}$ component of the electric field, i.e., $E_x(\mathbf{r})$, polarized longitudinally to the grating.

II. FORMULATION

To quantify this observation, we assume that the background refractive index of the material is n_0, and the grating is described by a sinusoidal modulation of the dielectric coefficient, so that $\epsilon(\mathbf{r})$ appearing in Eq. (1) is written as

*Electronic address: mookherjea@ece.ucsd.edu

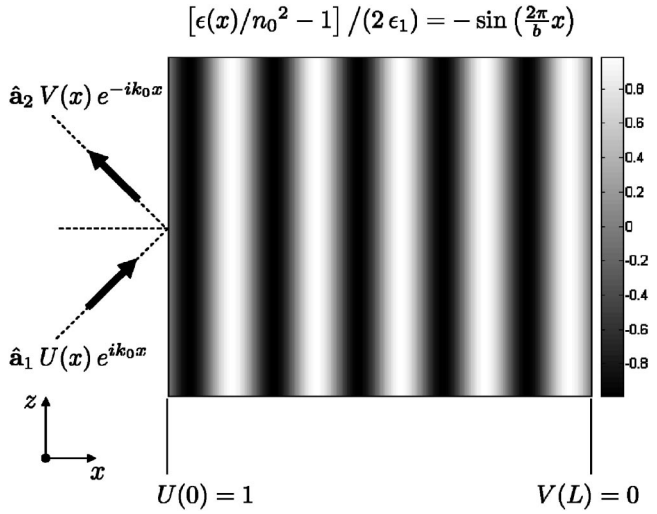

FIG. 1. Schematic of one-dimensional grating in the dielectric coefficient $\epsilon(x)$ with incident and reflected waves as indicated by Eq. (6). Also shown are the boundary conditions used in solved in the coupled-mode equations (8).

$$\epsilon(x) = n_0^2\left[1 - 2\epsilon_1 \sin\left(\frac{2\pi}{b}x\right)\right], \tag{3}$$

where $|\epsilon_1|$ is small compared to unity, but large enough that terms up to $O(\epsilon_1^2)$ are maintained. We obtain

$$\frac{1}{\epsilon}\frac{d\epsilon}{dx} \approx -2\epsilon_1\frac{2\pi}{b}\cos\frac{2\pi}{b}x - 2\epsilon_1^2\frac{2\pi}{b}\sin\left(2\frac{2\pi}{b}x\right),$$

$$\left[\frac{1}{\epsilon}\frac{d\epsilon}{dx}\right]^2 \approx 4\epsilon_1^2\left(\frac{2\pi}{b}\right)^2\cos^2\frac{2\pi}{b}x,$$

$$\frac{1}{\epsilon}\frac{d^2\epsilon}{dx^2} \approx 2\epsilon_1\left(\frac{2\pi}{b}\right)^2\sin\frac{2\pi}{b}x + 4\epsilon_1^2\left(\frac{2\pi}{b}\right)^2\sin^2\frac{2\pi}{b}x. \tag{4}$$

We write the field as $\mathbf{E}(\mathbf{r}) = \mathbf{A}(\mathbf{r})e^{i\beta z}$ and, after some straightforward algebra, we derive the following equation, accurate to $O(\epsilon_1^2)$,

$$\begin{aligned}0 = &\left(\frac{\partial^2}{\partial x^2} + \frac{\partial^2}{\partial z^2} + 2i\beta\frac{\partial}{\partial z}\right)\mathbf{A}\\ &+ \left(\frac{\omega^2}{c^2}n_0^2 - \beta^2\right)\mathbf{A} + n_0^2\frac{\omega^2}{c^2}\left[-2\epsilon_1\sin\frac{2\pi}{b}x\right]\mathbf{A}\\ &+ \hat{x}\left[2\epsilon_1\left(\frac{2\pi}{b}\right)^2\sin\frac{2\pi}{b}x\right]A_x - 2\epsilon_1\left(\frac{2\pi}{b}\right)\cos\frac{2\pi}{b}x\\ &\times[\nabla A_x + \hat{z}i\beta A_x] - 2\epsilon_1^2\left(\frac{2\pi}{b}\right)\sin 2\frac{2\pi}{b}x[\nabla A_x + \hat{z}i\beta A_x]\\ &+ \hat{x}\left[-4\epsilon_1^2\left(\frac{2\pi}{b}\right)^2\left\{\cos^2\frac{2\pi}{b}x - \sin^2\frac{2\pi}{b}x\right\}\right]A_x.\end{aligned} \tag{5}$$

Whereas the terms proportional to ϵ_1 vary spatially as $\cos(2\pi x/b)$, the terms proportional to ϵ_1^2 vary as $\cos(4\pi x/b)$ and $\sin(4\pi x/b)$, i.e., twice as rapidly. These terms arise from Eq. (2) and not from any Fourier-series expansion of $\epsilon(x)$—there is only a single "Fourier component" in Eq. (3).

The above equation, though conceivably suitable as the basis for numerical simulations, does not concisely state what sort of physical behavior is engineered by the new terms. To proceed further, we need an ansatz for **A**. We define $k_0^2 = n_0^2\omega^2/c^2 - \beta^2$, which has the following significance: if $\epsilon_1 = 0$ in Eq. (5), its solutions are $\mathbf{A}(x) = \hat{\mathbf{a}}\exp(\pm ik_0 x)$, where $\hat{\mathbf{a}}$ is a unit polarization vector.

Given a nonzero value for ϵ_1, we can expect different solutions: in this paper, we investigate the coupling between the two linearly-polarized components of the following field distribution:

$$\mathbf{A}(x) = \hat{\mathbf{a}}_1 U(x)e^{ik_0 x} + \hat{\mathbf{a}}_2 V(x)e^{-ik_0 x}, \tag{6}$$

where $\hat{\mathbf{a}}_1$ and $\hat{\mathbf{a}}_2$ are unit polarization vectors and U and V are scalar functions that describe the amplitudes. Clearly, the two components of Eq. (6) would be uncoupled when $\epsilon_1 = 0$, i.e., U and V would be independent of x. As an aside, we point out that Eq. (5) is linear and the principle of superposition holds; other families of field configurations may be important and can be considered in subsequent investigations, e.g., the Bloch function "principal components" [17] of the grating, as replacements for $\exp(\pm ik_0 x)$ in Eq. (6).

We assume that $U(x)$ and $V(x)$ are slowly varying over $2\pi/k_0$, so that

$$\begin{aligned}\frac{d^2\mathbf{A}}{dx^2} \approx &\hat{\mathbf{a}}_1\left(2ik_0\frac{dU}{dx} - k_0^2 U\right)e^{ik_0 x}\\ &+ \hat{\mathbf{a}}_2\left(-2ik_0\frac{dV}{dx} - k_0^2 V\right)e^{-ik_0 x}.\end{aligned} \tag{7}$$

This approximation can be restrictive in certain instances, and one should check that the obtained solutions satisfy this condition. The assumption may be relaxed if predominantly numerical analyses will be relied upon, giving up the convenience of closed-form analytical solutions.

Following the usual rotating-wave arguments [18,19], we divide the terms in Eq. (5) into two categories—(a) those that can be phase matched (exactly or with some detuning) to $\exp(ik_0 x)$ and hence contribute cumulatively to dU/dx and (b) those terms that can be phase matched to $\exp(-ik_0 x)$ can contribute cumulatively to dV/dx. We introduce the scalar coefficients $p_{12} \equiv \hat{\mathbf{a}}_1\cdot\hat{\mathbf{a}}_2$, $p_{xx} = (\hat{\mathbf{a}}_1\cdot\hat{x})(\hat{\mathbf{a}}_2\cdot\hat{x})$, $p_{zx} = (\hat{\mathbf{a}}_1\cdot\hat{z})(\hat{\mathbf{a}}_2\cdot\hat{x})$, and $p_{xz} = (\hat{\mathbf{a}}_1\cdot\hat{x})(\hat{\mathbf{a}}_2\cdot\hat{z})$ to write the resulting pair of differential equations as

$$\frac{dU}{dx} = \kappa^{(1)}Ve^{i2\delta^{(1)}x} + \kappa^{(2)}Ve^{i2\delta^{(2)}x}, \tag{8}$$

$$\frac{dV}{dx} = [\kappa^{(1)}]^* Ue^{-i2\delta^{(1)}x} + [\kappa^{(2)}]^* Ue^{-i2\delta^{(2)}x},$$

with the parameters defined in Table I.

Since $\delta^{(1)}$ and $\delta^{(2)}$ cannot both be zero simultaneously, there are two distinct phase-matching possibilities, (1) $k_0 \approx \pi/b$, which results in the conventional Bragg reflector design, and (2) $k_0 \approx 2\pi/b$, which requires a wavelength one-half that of the first case (i.e., at the second-harmonic optical

TABLE I. Coupling coefficient (κ) and phase mismatch parameter (δ) for the two reflection cases, defined so that the detuning parameter δ is zero at wavelength $\lambda = b/2$ and at $\lambda = b$, respectively, for a given value of b, the grating periodicity. The former case corresponds to the usual Bragg reflection and the existence of the second case depends on the longitudinal polarization of the field.

Case 1

$$\delta^{(1)} = \frac{\pi}{b} - k_0$$

$$\kappa^{(1)} = -\frac{\epsilon_1}{2k_0}\left\{\frac{\omega^2}{c^2}n_0{}^2 p_{12} - \left[\left(\frac{2\pi}{b}\right)^2 - k_0\frac{2\pi}{b}\right]p_{xx} - \beta\frac{2\pi}{b}p_{zx}\right\}$$

Case 2

$$\delta^{(2)} = \frac{2\pi}{b} - k_0$$

$$\kappa^{(2)} = -i\frac{\epsilon_1{}^2}{k_0}\left\{\left[\left(\frac{2\pi}{b}\right)^2 - \frac{k_0}{2}\frac{2\pi}{b}\right]p_{xx} + \frac{\beta}{2}\frac{2\pi}{b}p_{zx}\right\}$$

frequency) for a given grating (fixed value of b). Alternatively, in case (2), the wavelength may be kept constant if the spatial periodicity b is doubled (which is the situation we consider in the numerical calculations). Equation (6) with U and V as constant numbers representing fixed amplitudes is a solution of Eq. (5) when $\epsilon_1 = 0$. Note the field must have a longitudinal component, polarized along the grating axis, in order for $\kappa^{(2)}$ to be nonzero. It is also possible for both $\delta^{(1)}$ and $\delta^{(2)}$ to be nonzero, in general.

In order to solve Eq. (8), we need to impose suitable boundary conditions. Typically, we specify that the incident wave has amplitude $U(x=0)=1$ and require that the grating is long enough, with length L, such that there is zero amplitude for the "reflected" wave at the far-end of the grating $V(x=L)=0$. This is a reasonable assumption, since the reflected wave is itself generated per-unit-length from the incident wave, and this conversion is expected to have fully depleted the incident wave before the distance L. Consequently, the solution of Eq. (8) is well known in terms of hyperbolic trigonometric functions (Ref. [16], Chap. 6.6),

$$U^{(m)} = \frac{\delta^{(m)}\sinh[S^{(m)}(x-L)] + iS^{(m)}\cosh[S^{(m)}(x-L)]}{-\delta^{(m)}\sinh[S^{(m)}L] + iS^{(m)}\cosh[S^{(m)}L]}, \tag{9a}$$

$$V^{(m)} = \frac{i\kappa^{(m)}\sinh[S^{(m)}(x-L)]}{-\delta^{(m)}\sinh[S^{(m)}L] + iS^{(m)}\cosh[S^{(m)}L]}, \tag{9b}$$

where $(S^{(m)})^2 \equiv |\kappa^{(m)}|^2 - (\delta^{(m)})^2$ for $m=1$ or $m=2$. If S is real, the above solutions describe functions that are both exponentially decaying over $x=0$ to L, and hence describe a physical scenario where the incident wave, U, is continuously fed back into the reflected wave V as a function of x such that, at the input facet of the grating ($x=0$), $|U|^2 \approx |V|^2$, i.e., all the incident power has been converted into reflected power. Also, $|U|^2 + |V|^2$ is an exponentially decreasing function of x, since the field does not penetrate very far into the grating if it is being reflected.

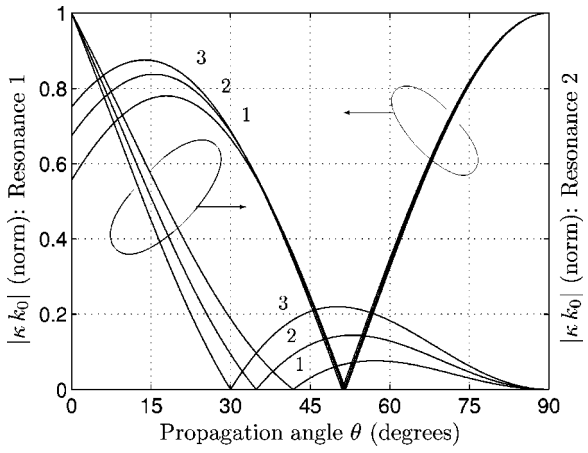

FIG. 2. Magnitude of the contradirectional coupling coefficients (multiplied by k_0 and normalized to unit peak value; units μm^{-2}) for the two Bragg reflection cases. Numerical values: $\lambda_0/n_0 = 1$ μm and $b = 1.5$, 1.75, and 2.0 μm, labeled by "1," "2," and "3," respectively.

In general, the overall phase of each κ depends on the choice of reference plane, but there is a relative shift of $\pi/2$ in the phase of κ between the two cases, i.e., $|\text{phase}(\kappa^{(1)}) - \text{phase}(\kappa^{(2)})| = \pi/2$, which is important for the round-trip resonance condition for waves propagating between two such reflectors. For TE polarized waves, $p_{xx} = p_{xz} = 0$ and $p_{12} = 1$, and the conventional results are unmodified [16]. For the TM polarization, if we assume that the two waves in Eq. (6) propagate at angles $\pm\theta$ with respect to the z axis, we calculate that $p_{12} = -\cos 2\theta$, $p_{xx} = -\cos^2\theta$, $p_{zx} = -\sin\theta\cos\theta = -p_{xz}$, $k_0 = (2\pi n_0/\lambda_0)\sin\theta$, and $\beta = (2\pi n_0/\lambda_0)\cos\theta$, where λ_0 is the wavelength in vacuum corresponding to ω. Consequently, changing the wavelength λ_0 and changing the amgle θ have similar effects in the following calculations. Since k_0 appears in the denominator of κ, and $1/k_0 \to \infty$ as $\theta \to 0$, it is convenient to instead graph the product of κ and k_0. (This follows simply from the fact that the grating is along x whereas θ is defined from the z axis.) Defining $\lambda = \lambda_0/n_0$, we obtain the relationships

$$k_0\kappa^{(1)} = -\frac{\epsilon_1}{2}\left[\left(\frac{2\pi}{\lambda}\right)^2\cos 2\theta - \frac{2\pi}{b}\cos^2\theta\left(\frac{2\pi}{b} - 2\frac{2\pi}{\lambda}\sin\theta\right)\right], \tag{10a}$$

$$k_0\kappa^{(2)} = -i\epsilon_1{}^2\frac{2\pi}{b}\cos^2\theta\left(\frac{2\pi}{b} - \frac{2\pi}{\lambda}\sin\theta\right) = 0 \quad \text{if } \delta^{(2)} = 0. \tag{10b}$$

These coefficients are plotted as a function of θ in Fig. 2 for

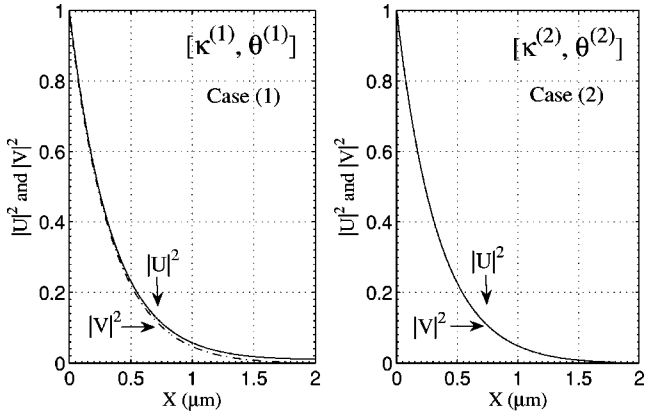

FIG. 3. Numerically calculated *E*-field envelopes of the forward propagating (*U*: continuous line) and reflected (*V*: dashed line) fields, showing that the incident field is reflected almost completely in the given length of the grating. The wavelength is the same in both cases, and the grating period is doubled in case (2), compared to case (1), and the angles of incidence are different in the two cases. Numerical values of parameters are given in the text.

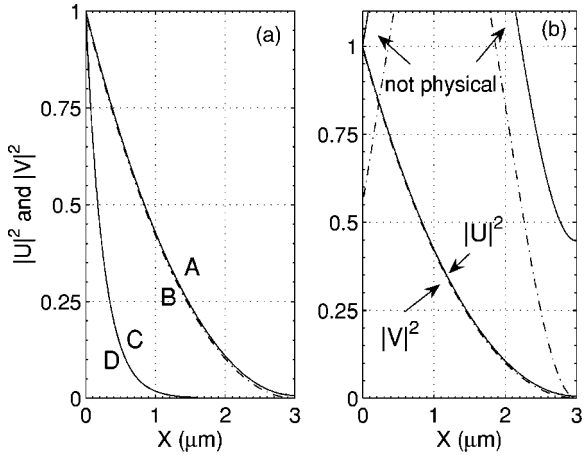

FIG. 4. (a) Reflection is observed for both cases (1) and (2), with reference to Table I. Numerical calculations of the incident-wave envelope *U* (continuous lines A and C) and the reflected-wave envelope *V* (dashed lines B and D), where C and D refer to conventional Bragg-reflection (case 1) and A and B refer to reflection according to case 2. (b) For a different value of ϵ_1, $[S^{(1)}]^2$ is a negative number and the fields in Eq. (9a) do not exponentially decay with *x*; hence the incident wave is not reflected according to case 1; however, the wave is still reflected according to case 2.

three different values of *b*, given λ. As $\theta \to 90°$, the waves propagate predominantly along the *x* axis, and by definition of the Poynting power flow, the waves are no longer polarized longitudinally to the grating ($p_{xx}=p_{zx}=0$); hence $\kappa^{(2)}$ vanishes. The limit $\theta \to 0$ is not valid in this simple theoretical formulation.

When the Bragg resonance condition for $\kappa^{(2)}$ is satisfied (i.e., $\delta^{(2)}=0$), the magnitude of $\kappa^{(2)}$ is (algebraically) zero, as shown by the three nulls between 30° and 45° in the curve for "resonance 2" in Fig. 2. This coupling coefficient reaches a peak value *away* from what is usually considered as the Bragg resonance condition for contradirectional coupling, as shown in Fig 2.

III. NUMERICAL CALCULATIONS

The prediction that a second-reflection condition can exist between the two fields of Eq. (6) is validated with numerical solution of the differential equations. (Simulation algorithms which do not explicitly enforce the divergence condition are unsuitable for this task.) We have used two numerical techniques, (1) a shooting method based on a fourth-order Runge-Kutta propagator and (2) a finite-difference (polynomial-based collocation) method, and which generates the data shown in Fig. 3.

The wavelength of $\lambda_0=1.5$ μm in a dielectric with refractive index $n_0=3.5$ is used, with $\epsilon_1=0.225$. Based on Fig. 2, the two reflection conditions exist for different regimes of the propagation angle, θ. For case (1), which is based on Bragg reflection of the transverse field component, the angle θ should be large, so that the field is mostly polarized transverse to the grating, and we pick $\theta^{(1)}=75.0°$ and a grating period $b=221$ nm to satisfy the Bragg resonance condition, i.e., $\delta^{(1)}=0$. Over a distance of 2 μm, a fraction $|V(0)/U(0)|^2=98.9\%$ of the incident power is reflected. In case (2), we leave the wavelength unchanged and set the grating period $b=442$ nm [twice that in the case (1) as suggested earlier]. Since the leading-order term in $\kappa^{(2)}$ is $O(\epsilon_1{}^2)$, we (heuristically) pick a value for $\epsilon_1=0.45$, twice as large as earlier. Since it is the longitudinal field component that is significant in this case, the field should therefore be incident at a different angle to the grating than in case (1). For $\theta^{(2)}=10.8°$, and over a distance of 2 μm, the numerical simulation shows almost full power reflection in this case as well.

IV. DISCUSSION

We have shown earlier that $\kappa^{(2)}=0$ if $\delta^{(2)}=0$, but for reflection of the incident field, we require that both *U* and *V* decrease exponentially with *x*. If $S^{(2)}$ in Eq. (9) is to be a real number, it is necessary that

$$|\kappa^{(2)}| > |\delta^{(2)}|, \quad \text{i.e.,} \quad \frac{b}{2\pi/k_0} < \epsilon_1{}^2 \cos^2\theta^{(2)}, \tag{11}$$

which restricts $b \leqslant \lambda/4$ in all cases. For weak gratings, e.g., $|\epsilon_1| \approx 0.1$, Eq. (11) prescribes a grating period in the nanometer scale (for optical wavelengths), which is difficult to realize with lithographic fabrication techniques. Stronger gratings are necessary to observe macroscopically the effects of these longitudinal terms in the wave propagation equation. However, a composite material comprising alternating layers of titanium-dioxide and a nonlinear polymer, which has shown a large third-order nonlinear susceptibility [20], is characterized by layer thicknesses in the tens of nanometers, and may be a suitable material for experimental studies. Interestingly, the theory for this enhanced nonlinearity [21] is valid in the same range of layer thicknesses, $b \leqslant \lambda/4$, as the present theory of longitudinal field reflection, i.e., when the phase accumulated by a wave in propagating across a single layer of the multilayer stack or a single halfperiod of the grating is less than $\pi/2$.

Furthermore, if b is chosen according to the above relationship, it follows from the definitions in Table I that

$$\delta^{(2)} > \frac{2\pi}{b}(1 - \epsilon_1{}^2 \cos\theta^{(2)}) \approx \frac{2\pi}{b} \quad \text{if } |\epsilon_1| \ll 1. \quad (12)$$

Examining Eq. (9b), we see that near-unity reflection is achieved when, first, $|\kappa^{(2)}L|$ is greater than 1, and secondly, when $|\kappa^{(2)}|^2$ is only slightly greater than $(\delta^{(2)})^2$, so that $S^{(2)}$ is a small real number.

Values of the parameters may be chosen so that, when the conditions for reflection in case (2) are satisfied, conditions for reflection according to case (1) may or may not simultaneously be satisfied. For example, Fig. 4 shows examples where a field of wavelength of $\lambda_0 = 2\ \mu$m propagates with angle $\theta = 7.5^\circ$ in a dielectric (glass) with refractive index $n_0 = 1.50$, and with $\epsilon_1 = 0.380$ and $\epsilon_1 = 0.364$ in the two cases, respectively. In the case of Fig. 4(a), both conditions $|\kappa^{(1)}| > \delta^{(1)}$ and $|\kappa^{(2)}| > \delta^{(2)}$ are satisfied, and the reflection coefficients for λ and $\lambda/2$ are 99.9 and 98.3 %, respectively. In the case of Fig. 4(b), however, $|\kappa^{(1)}| < \delta^{(1)}$ while $|\kappa^{(2)}| > \delta^{(2)}$, so reflection exists only in case 2. The conventional theory would predict that we are outside the stopband of the grating filter, whereas the role of the longitudinal field may result in strong reflection, instead. Values of κL in both cases are in the range of 5–10, for which coupled-mode theory is reasonably accurate, generally to within 10–20 % of results computed from an *ab initio* numerical method [22]. Further numerical studies, based on Eq. (5), will be carried out to develop a deeper understanding of these novel effects, and especially the role of the second-order x derivatives on U and V in Eq. (8).

V. CONCLUSION

We have derived the wave propagation equation in a one-dimensional periodic medium characterized by a sinusoidal variation in the dielectric coefficient along the transverse axis. We have shown that consideration of the longitudinal field component reveals a second-resonance Bragg reflection, which condition exists for waves that have a field component polarized parallel to the axis of the grating. To investigate this observation in a framework that yields closed-form solutions, we have used coupled-wave theory, supplemented with numerical calculations, to provide a simple comparison with the conventional results.

ACKNOWLEDGMENTS

The authors are grateful to Jacob Scheuer (Caltech) for insightful comments and useful criticism. This work was supported by the National Science Foundation and the Helleman Program at UCSD.

[1] H. Kogelnik, Bell Syst. Tech. J. **48**, 2909 (1969).
[2] A. Yariv, IEEE J. Quantum Electron. **QE-9**, 919 (1973).
[3] K. Wagatsuma, H. Sakaki, and S. Saito, IEEE J. Quantum Electron. **QE-15**, 632 (1979).
[4] D. G. Hall, in *Progress in Optics*, edited by E. Wolf (Elsevier, The Netherlands, 1991), Vol. XXIX, pp. 1–63.
[5] T. K. Gaylord and M. G. Moharam, Proc. IEEE **73**, 894 (1985).
[6] N. Izhaky and A. Hardy, J. Opt. Soc. Am. A **15**, 473 (1998).
[7] P. Paddon and J. F. Young, Opt. Lett. **23**, 1529 (1998).
[8] L. Novotny, M. Beversluis, K. S. Youngsworth, and T. G. Brown, Phys. Rev. Lett. **86**, 5251 (2001).
[9] W. E. Moerner and M. Orrit, Science **283**, 1670 (1999).
[10] M. O. Scully and M. S. Zubairy, Phys. Rev. A **44**, 2656 (1991).
[11] S. Quabis, R. Dorn, M. Eberler, O. Glockl, and G. Leuchs, Opt. Commun. **179**, 1 (2000).
[12] J. W. M. Chon, X. Gan, and M. Gu, Appl. Phys. Lett. **81**, 1576 (2002).
[13] M. Lax, W. H. Louisell, and W. B. McKnight, Phys. Rev. A **11**, 1365 (1975).
[14] A. Ciattoni, P. Di Porto, B. Crosignani, and A. Yariv, J. Opt. Soc. Am. B **17**, 809 (2000).
[15] U. Levy, C.-H. Tsai, L. Pang, and Y. Fainman, Opt. Lett. **29**, 1718 (2004).
[16] A. Yariv and P. Yeh, *Optical Waves in Crystals* (Wiley, New York, 1984).
[17] C. M. de Sterke and J. E. Sipe, Phys. Rev. A **38**, 5149 (1988).
[18] F. Bloch and A. Siegert, Phys. Rev. **57**, 522 (1940).
[19] P. L. Knight and L. Allen, Phys. Rev. A **7**, 368 (1973).
[20] G. L. Fischer, R. W. Boyd, R. J. Gehr, S. A. Jenekhe, J. A. Osaheni, J. E. Sipe, and L. A. Weller-Brophy, Phys. Rev. Lett. **74**, 1871 (1995).
[21] R. W. Boyd and J. E. Sipe, J. Opt. Soc. Am. B **11**, 297 (1994).
[22] L. A. Coldren and S. W. Corzine, *Diode Lasers and Photonic Integrated Circuits* (Wiley, New York, 1995).